energy&fuels

pubs.acs.org/EF Article

Integration of Thermal Treatment and Extrusion by Compounding for Processing Various Wastes for Energy Applications

Shreyas S. Kolapkar, Stas Zinchik, Zhuo Xu, Armando G. McDonald, and Ezra Bar-Ziv*

Cite This: *Energy Fuels* 2021, 35, 12227−12236 Read Online

ACCESS | Metrics & More | Article Recommendations | Supporting Information

ABSTRACT: Waste generation is increasing, and a significant portion of the wastes is being landfilled. Torrefaction of such wastes to produce clean fuels is one of the potential solutions. This paper studied torrefaction of mixed fiber−plastic wastes at 300 °C in an integrated torrefaction−extrusion screw reactor with a throughput of up to 70 kg/h. The study experimentally measured the thermomechanical properties of the torrefaction−extrusion process and the pellets produced. The study presents the results for thermal dynamics, the effect of shaft configuration on residence time, specific mechanical energy (SME), heat transfer coefficient (U), specific heat (C) of mixed wastes, and mechanical and rheological properties of pellets. First, the thermal dynamics of the system were studied along the corresponding response of heaters with and without the flow of materials measured. The residence time measurement showed 20% and 40% cut flighting had about 2.3 and 3.7 times more residence time compared to a regular screw. The specific heat of the heterogeneous mix blend was measured at 1.58 kJ/(kg °C). The average overall heat transfer coefficient was measured experimentally for the reactor at 52.5 W/(m^2 °C). The correlation between specific mechanical energy and mass flow showed more than 3 times decrease in specific energy consumed when the feed rate was increased from ∼10 to 50 kg/h. Thermomechanical analysis, flexural testing, and rheological testing were performed on the produced pellets to measure pellet properties.

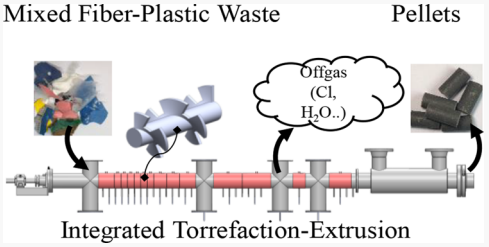

1. INTRODUCTION

In 2017, the US generated about 120 million tons of fiber (paper, paperboard, and wood) and plastic wastes combined, of which 58.31 million tons was landfilled.[1] With increased waste generation and 2.6% annual reduction in US landfill capacity, the US is anticipated to have only 10−15 years of landfill capacity remaining by the year 2021.[2] In parallel, based on the current five-year trend, the average year-over-year tipping fees paid by the consumer have steadily increased by 2.8% since 2016 with the US national average at $53.72/ton for year 2020.[3] There are numerous additional challenges like the Chinese ban[4,5] on US plastic waste import, lack of markets for recycled materials, lack of producer responsibility, lack of recycling, and composting opportunities for consumers.[6] All these challenges have created a sense of urgency to address the waste treatment challenge.

To treat and valorize these wastes, one of the pathways is thermal treatment. Thermal treatment technologies like torrefaction, pyrolysis, and gasification have widely been explored as sustainable and economical pathways and also as alternatives to traditional landfilling.[7,8] The current study focuses on torrefaction, a mild thermal treatment process in an oxygen-free or drastically reduced oxygen environment.[9] The main product for the torrefaction is the solid fraction, which can be used in power and heat application.[10] Various types of reactor technologies like rotating drum, screw, multiple hearth furnace (MHF), fluidized bed, belt and vibrating grate, and microwave reactor have been developed and are used for carrying out these thermal processes.[9,11] These thermal treatment technologies have been extensively used and tested with biomass as a feedstock at various scales.[11] As our technology integrates torrefaction with extrusion (and pelletization), the following paragraph discusses the pelletization process in the biomass/wood pellet industry. The typical pellet production process involves four key steps: (i) collection and debarking (for wood), (ii) grinding of the feedstock, (iii) drying, and (iv) pelletization. The pelletization is done by using various different methods like the hot press, briquetting, and most commonly pellet mills.[12,13] For fiber−plastic waste pellets production, the current state-of-the-art technologies are similar to the biomass and wood pellet industry and most commonly involves the use of pellet mills to produce pellets. Applications of the fiber−plastic pellets include (i) use as a feedstock for upgrading[14,15] to liquid transportation fuels and sustainable aviation fuels using pyrolysis or gasification and (ii) solids fuels for use in cement kilns or small power plants.[16−18] The mixed waste plastic (with no to little fibers) pellets also find applications in the production of polymer alloys or

Received: June 8, 2021
Revised: July 16, 2021
Published: July 27, 2021

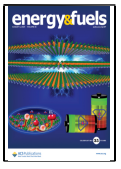

composites materials for producing items like shingles and construction blocks.

Converse to the traditional biomass and wood pelleting industry, with the use of wastes containing various plastics waste streams, traditional technologies face technical challenges like (i) batch-to-batch inconsistencies, (ii) heterogeneities within the waste stream, (iii) difficulties in conveying and bridging due to the low density (∼50 kg/m^3), and (iv) extreme difficulties in feeding and extruding mixed fiber plastics. All these factors impose techno-economic barriers in recycling and the development of waste treatment technologies. To address the technological challenges with the use of fiber−plastic wastes and to meet the needs of the heat and power industry, our team developed a torrefaction−extrusion system using a modified screw reactor. Screw reactors have been studied for several decades, especially in the plastic extrusion industry.[19] Several past studies also have explored its use with various types of biomass and similar materials. Kelkar et al.[20] used spent coffee grounds in a single auger reactor at a federate of 1−1.5 kg/h. Atienza-Martínez et al. used a lab-scale auger reactor to torrefy sewage sludge.[21] Zinchik et al. tested 10 different biomass types in a screw reactor with a feed rate of 0.1 kg/h.[22] Brown et al. developed a lab-scale auger reactor for biomass fast pyrolysis using red oak.[23] Numerous such studies[9,22−26] have been performed by using a screw or auger reactor along with several others reviewed in detail by Brown et al.[23] and Campuzano et al.[11] However, almost all these studies mainly focus on biomass material with heat transfer material and have standard screws designs (unmodified) with separate or no compaction process. This study used a screw, modified with cuts in the flights, to produce torrefied pellets from fiber−plastic waste material. The integration of this modified screw design for torrefaction with an extruder used for compaction and pelletization is a novel system and has not been studied before. The current study focuses on this fiber−plastic waste stream that is common in the Material Recovery Facility (MRF) and Refused Derived Fuel (RDF) pellet industry. It also broadly applies to any waste stream that contains organic wastes and plastics. We studied various blend ratios of fiber−plastic wastes. However, as the 60% mixed fiber waste and 40% mixed plastic waste blend was studied extensively for the onstream operation of ∼700 h, it is presented as a case study to demonstrate the properties of the pilot system and the products. This study also aims to shed light on the above topics and provide heat dynamics of a screw torrefaction system, the heat capacity of the fiber−plastic blend, specific energy consumption, and the relation between residence time and screw configuration.

The properties of the final torrefied product are often dictated by the incoming material properties and the extent of torrefaction. The extent of torrefaction is governed by two key factors: reaction kinetics and heat transfer. Reaction kinetics along with waste dechlorination mechanisms has been studied for the fiber−plastic blends in the team's previous studies[22,27,28] and will not be discussed. For studying heat transfer, it is important to obtain heat transfer dynamics and specific heat of the material. Heat transfer dynamics are dependent on the system configuration, type of material, and scale of the process. Out of these parameters, scale and configuration of the system configuration remained fixed during the study, but despite the presence of a large database for the heat capacity of various materials, the measurement of heat capacity is challenging as the material used is heterogeneous in nature and changes from batch to batch. To model the actual temperature of the material inside the reactor, heat capacity measurement is essential for every batch. An experimental method to measure the heat capacity of the material blend was developed in this study.

This study also attempts to experimentally measure various other thermomechanical properties of the material and the system. The other key properties that were measured are the heat transfer coefficient of the system, the residence time for different configurations, specific mechanical energy, and material properties like density, pellet durability, thermomechanical analysis (TMA), rheology, flexural strength and modulus, and FTIR characterization. Current literature on the heat transfer coefficient and specific energy is presented below.

The experimental measurement of the heat transfer coefficient is challenging due to the dynamic nature and moving components of screw reactors. Some simulation efforts have been made by using the Eulerian method[29] or the discrete elements method[30] (DEM) to model mass and heat transfer in screw reactors. Funke et al.[31] simulated heat transfer in a twin-screw auger type reactor using biomass and heat carrier material and observed its strong dependence on mixing quality and the ratio of heat carrier to biomass particles. This simulation study claimed to achieve heat transfer coefficients in the range of 150−350 W/(m^2 K), comparable to a fluidized bed reactor. Qi et al.[32] developed a heat transfer model using DEM in a double-screw reactor and reported total heat transfer coefficients between 70 and 100 W/(m^2 K) depending on various operating conditions. Waje et al.[33] studied the thermal performance of a screw dryer and found an overall heat transfer coefficient between 46 and 102 W/(m^2 K). Thus, there is a large variability of heat transfer coefficient predictions is made by the simulation (between 46 and 350 W/(m^2 K)) studies, largely due to a several assumptions made for simplification purposes during the modeling. Also, most of these studies simulate a small lab scale (≤3 kg/h) system with twin screws and the use heat transfer materials. The current study attempts to experimentally measure heat transfer coefficient in a single-screw reactor at a larger scale (up to 70 kg/h) in the absence of heat transfer material.

The specific extrusion energy or specific mechanical energy (SME) is the amount of mechanical energy required to carry out the extrusion process; specifically, it is work input from the drive motor into the material being extruded.[34] SME is an important process parameter that influences product characteristics like density and material hardness[35] and depends on multiple process parameters like viscosity, screw speed, barrel temperature, moisture, material type, average material size, and configuration of the screw.[34−37] Several studies have reported SME for twin-screw auger reactors: Godavarti et al.[34] reported 43−67.8 kWh/t for cornmeal material in a twin-screw reactor (length/diameter (L/D) = 28.6) at 16.5 kg/h. Schmid et al.[36] reported 122 ± 5 to 222 ± 10 kWh/t for chokeberry pomace powder in a 26 mm diameter corotating twin-screw reactor (L/D = 29) at 10 kg/h and 200−800 rpm. Sasimowski et al.[37] derived the empirical correlation of SME = 2221.4 − 13.027n + 0.034n^2, where n is rpm of extruder. The study reported a 45% decrease (474 to 260 kWh/t) in SME with a 4-fold increase in rpm from 50 to 200 rpm for the poly(butylene succinate)−wheat bran blend in a twin-screw reactor (L/D = 40) with material temperature ranging from 123 to 155 °C. Based on the literature review, very few SME studies are

https://doi.org/10.1021/acs.energyfuels.1c01836
Energy Fuels 2021, 35, 12227−12236

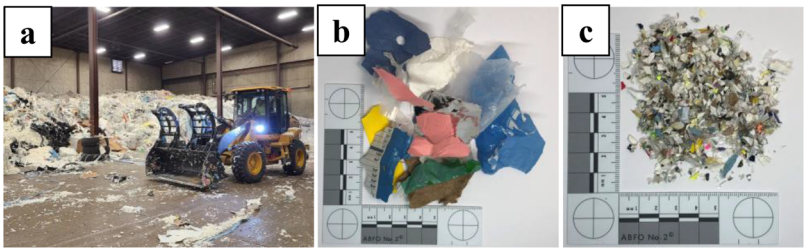

Figure 1. Various stages of the fiber−plastic waste preprocessing and corresponding particle sizes: (a) tipping-floor stage where fibers and plastics are blended (≥300 mm); (b) shredding stage 1 (≤50 mm); (c) shredding stage 3 (≤3 mm).

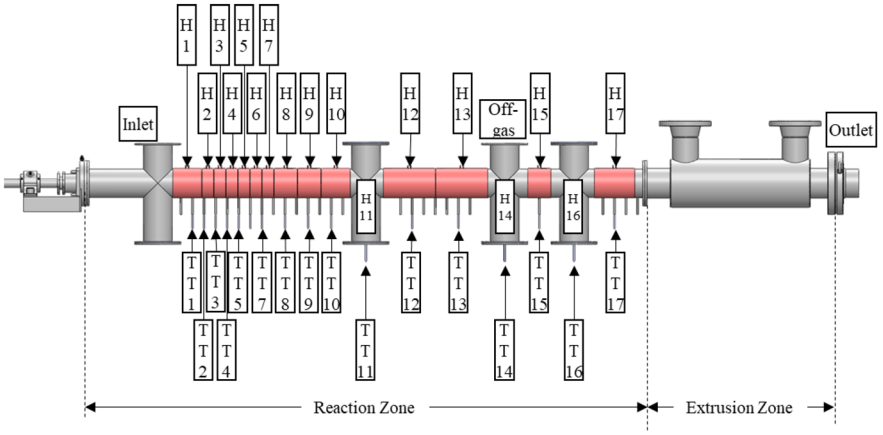

Figure 2. Integrated torrefaction−extrusion system showing the heaters (H1 to H14) and thermocouples (TT1 to TT17).

performed on single-screw reactors with fiber−plastic waste as a feedstock.

The residence time measurement is the time spent by the material in the reactor. The residence time in a regular screw is approximately given by the residence time equation $t_{res} = c/\nu$, where c and ν are the number of pitches in the screw and rotation frequency, respectively.[22] However, because of the complex geometry of the modified screw (paddle) used in the study, it is difficult to predict the exact residence time of the material. Various approaches have been developed in the past to predict the residence time of material in complex screw designs, some of which are as follows. Zinchik et al. used the approach of calculating the effective number of pitches followed by curve fitting the data for numerous experiments to calculate the residence time.[22] Lepschi et al. used fluorescence spectroscopy to measure the residence time and residence time distribution in the corotating twin-screw reactor,[38] while Nikitine et al. calculated the residence time using $t_{res} = \tau\rho V/M$, where τ is the fill rate, ρ is the density, V is the extruder "free" volume, and M is the mass flow rate and developed a model to predict the distribution.[39] In this study, the measurement was simplified and the residence time for various screw configurations was measured experimentally based on the observation of the power consumption data. More details about the approach are presented in section 2.2.

The previous works[10,22,27,40] by the team studied torrefaction from the microgram to a few grams scale and developed a detailed understanding of reaction kinetics, chlorine removal in the torrefaction, material properties of the feedstock, and pellets. Based on these studies, a large size torrefaction system with throughput up to 70 kg/h was developed. This study presents the thermomechanical test results from hundreds of hours of operation performed on the system.

2. MATERIALS AND METHODS

2.1. Material Identification and Preparation. The fiber−plastic waste material used in the experiments was supplied by Convergen Energy (CE) LLC. The waste blend used is a fiber−plastic waste blend with 40% mixed plastic and 60% fiber (paper and cardboard). To identify the exact types of fiber/plastics in the feedstock, FTIR analysis was conducted on the incoming materials. Analysis was carried on 30 randomly chosen pieces using an FTIR spectrometer (Thermo-Scientific Nicolet Summit Pro) with an attenuated total reflection (ATR) accessory (ZnSe crystal, iD5). OMNIC V9 software, plastic standards (low-density polyethylene (LDPE) from Rainer Plastics, Inc., high-density polyethylene (HDPE) from Equistar Petrothene LB01000, and polypropylene (PP) from Amcor), and Aldrich, Hummel, and Nicolet spectral libraries were used to analyze the data.

The blend is mainly comprised of paper, laminated paper, label matrix residuals, laminated nonrecyclable papers, and a wide mix of plastics including LDPE, HDPE, PP, poly(ethylene terephthalate) (PET), and traces of polyamides (nylon). More details are provided in section 3.

Figure 1 shows various stages in the feedstock preparation process for the above-described blend. The waste feedstock which consists of paper and plastic was hauled separately to the tipping floor from the various generation sources. The separate paper and plastic were then mixed in a ratio of 60:40 by using the loader as shown in Figure 1a. Ferrous and nonferrous metals were then removed from the blend before the shredding processes. The material was shredded by using a two-stage shredding process. In stage 1, the material was shredded by a series of common industrial shredders to a size of ≤50 mm. In stage 2, final shredding was performed in-house using a cross-cut shredder (Allegheny, model 16-75CX) to a size of ≤3 mm. The final stage shredding is performed at comparatively low speeds (<200 rpm) as high-speed shredding (>1000 rpm) tends to cause fluffing up of the material.

The typical shredded material bulk density ranged from 50 to 70 kg/m^3. The moisture content ranged between 1.4% and 5.5%. More details regarding the material such as proximate analysis, ultimate

https://doi.org/10.1021/acs.energyfuels.1c01836
Energy Fuels 2021, 35, 12227−12236

analysis, ash content, and fusion temperatures are provided in the previous study[27] and are summarized in Appendix I of the Supporting Information. These properties are average results of tests carried over a several-year period at CE's production facility.

2.2. Equipment. Figure 2 shows the reactor−extruder setup used for the experiment. The total combined length of reactor and extruder is 3.3 m. The system consists of a single shaft with different zones, defined by different function-specific flights mounted on it. In the reaction zone, the flights are modified with cuts to increase the residence time. The reaction zone has an L of 2.67 m and a D of 101.6 mm with a paddle (screw) pitch of 76.2 mm. The flights in the extruder section are modified to have a decreasing variable pitch to achieve the compaction required for the formation of pellets. There are a total of 12 flights in the extruder section starting with 76.2 mm and gradually decreasing to 25.4 mm. The L/D ratio of the extruder section is 6, which is smaller as compared to typical modern extruders L/D ratios of 18−40.[41] Shorter L/D allows for lower torque and power requirements.[41] There are four access ports to the reactor, each with top and bottom access. Port 1 top (from left) is used as an inlet to the reactor, and port 3 top is used to send off-gases to the condensers and gas cleanup system (not shown). The rest are used for maintenance access. The material is thermally treated in the reactor section and continues into the extrusion section, which is 101.6 mm in D and 102.4 mm in total L. At the end of the extruder, the material is extruded in the form of long rods by using a die with 8 holes of 12.7 mm D each. The extruded rods are cut into pellet form by using the cutter attached to the die (not shown). Two shafts were used in this study, first with 20% cuts and 40% cuts. The latter was used only for residence time study as described in section 2.3.3.

The reactor is heated by using a series of electric band heaters. All the band heaters are operated at 480 V and have a capacity ranging from 2 to 5 kW. The heaters are configured in five sets as follows: (a) set 1, located between ports 1 and 2, consists of 10 heaters of total 30 kW in a sequence of 1 × 5 kW, 6 × 2 kW, 2 × 4 kW, and 1 × 5 kW; (b) set 2, located between ports 2 and 3, consists of two heaters of total 9 kW; (c) set 3, located between ports 3 and 4, consists of one heater of total 4 kW; (d) set 4, located after port 4, consists of 1 heater of total 6.5 kW; and (e) set 5 consists of three heaters in the access port bottoms with 2.5 kW each. The distance of heaters H1 to H17 from the center of the inlet port is 0.19, 0.24, 0.29, 0.34, 0.39, 0.44, 0.5, 0.56, 0.60, 0.70, 0.83, 0.98, 1.21, 1.44, 1.59, 1.69, and 1.84 m, respectively. The extruder temperature was precisely controlled by using an air-cooled heat exchanger jacket. The oxygen-free environment is maintained by (a) by using a mechanical airlock on the inlet side, (b) a material seal created by the extruder on the outlet side, and (c) flowing nitrogen at ∼4.7 L/min. All the condensable and noncondensable gases produced during the process are sent to a conditioning system consisting of dry sorbent injection, condensers, and demister filter attached to port 3 of the reactor−extruder system (not shown). The material was metered by using a volumetric feed auger equipped with a hopper.

All the process data were acquired by using Automation Direct - Productivity 3000 PLC and Aveva Indusoft Web Studio HMI ver. 8.1. All the process parameters like thermocouple temperature (TT1 to TT17), duty cycles of the heaters, pressures, motor rotation speeds, motor load, and so on were measured in real time at an acquisition rate of one measurement per second.

2.3. Experimental Procedures. *2.3.1. Mass Flow Rate.* The mass flow rate was measured automatically by using four load cells attached to the pellet cooling unit at the outlet. The load cells were calibrated before the experiments. The weight was measured continuously with a resolution of 0.1 g. The experiment was repeated for various rotation frequencies of the feed auger from 0 to 16 rpm.

2.3.2. Thermal Dynamics. To understand the stability of the system, thermal dynamics were measured for several hours. The PID parameters of the heaters were optimized to minimize the overshoot of the temperatures. The heating was started at the set point temperature of 300 °C with a typical ramp-up time between 4 and 8 h. After the set temperature was reached, the system was maintained at a steady-state for a minimum of 2 h to ensure all the components have reached the set point. All the temperatures were within ±1 °C of the set point temperatures. The data for heat losses used in other heat transfer calculations were collected at this point. The material feed into the reactor and the dynamic response of the system was recorded.

2.3.3. Residence Time. In the reactor, the relevant residence time is from the inlet to the point where the material flows into the extruder. As the screw had cuts, it was not possible to theoretically calculate the residence time by using the standard formulas for the screw. A new method based on observation of the reactor motor power behavior was developed for the measurement. When the material reaches the extruder zone, there is an increase in the power of the motor rotating the shaft which is indicative of the material entering the extruder. Because the reaction zone is free of any compaction units, the motor load can only increase once the material reaches the extrusion zone. The experiment was performed as follows: (a) the feed auger motor was turned off; (b) the reactor motor was rotating continuously at a given set point; (c) the feed auger was turned on at a given frequency and then turned off at a predetermined time interval; (d) the reactor was emptied by monitoring the reactor motor load (return to load values recorded in step b. After a given experiment, the rotation frequency of the reactor motor was changed, and steps a−d were repeated. Details regarding the interpretation of plots are provided below. As there are cuts in the screw that delayed the material movement, it is expected that more cuts would result in a longer residence time. The experiment was repeated for screw with 20% cuts and 40% cuts. The percent cut is calculated by the formula in eq 1.

$$\text{cut (\%)} = 1 - \frac{\text{area of paddle}}{\text{area of full screw}} \quad (1)$$

Figure 3 shows the typical measurement for the residence time. In the reactor configuration shown in Figure 2, the residence time is denoted as the time required for the material to travel from the inlet of the reactor to the start of the extruder. As it is difficult to predict the exact residence time by using the conventional method of timing the material feed from inlet to outlet due to the integration of screw and extruder as well as cuts on the screw and variability in material densities, the method described above was used. As seen for the measurement in Figure 3, initially the feed auger is off as seen from the 0% feed motor load, and the reactor is operating at a normal load of ∼33% motor load. At 1 min, the feed motor is turned on, represented by the rise in the feed motor curve (orange); meanwhile, the reactor motor load continues to be maintained at 33% showing the resistance-free travel of material in the reactor zone. At 3 min, the reactor load curve (blue) rises signaling that material has reached the extruder. As defined earlier, this time from 1 to 3 min is thus defined as the residence time. After some time, the feed auger was stopped as represented by the drop in the feed motor load curve and resulting fall of the reactor motor load. This process is repeated several times by changing the reactor shaft speeds.

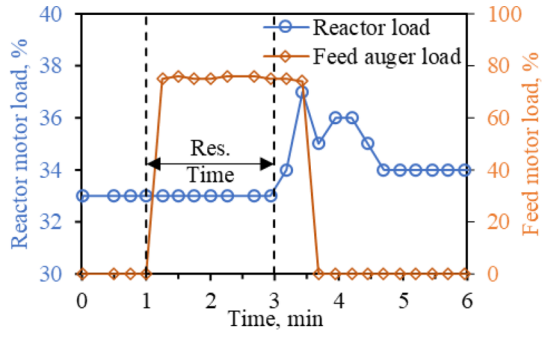

Figure 3. Reactor and feed motor load vs time showing the measurement procedure of residence time.

2.3.4. Specific Heat. The specific heat was calculated based on eq 2

https://doi.org/10.1021/acs.energyfuels.1c01836
Energy Fuels 2021, 35, 12227−12236

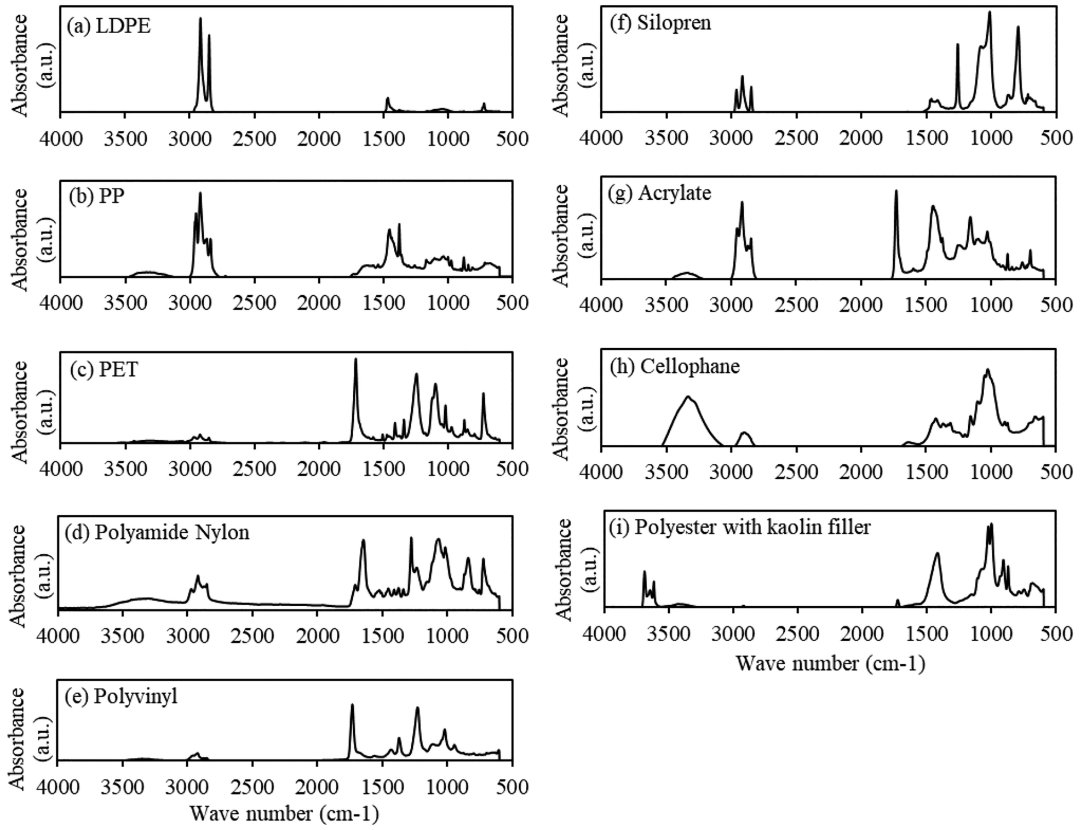

Figure 4. Infrared spectra of various materials identified in waste feedstock showing various plastic polymers, rubbers, and fibers. Polymers: LDPE, PP, PET, polyamide nylon, poly(vinyl acrylate), polyester with kaolin filler. Rubber: Silopren. Fiber: cellophane/cellulose.

$$c = \frac{q}{\dot{m}(T_{out} - T_{in})} \tag{2}$$

where T_{out} is the temperature of the material exiting the reactor and T_{in} is the environmental temperature. First, the specific energy, $q/\dot{m}$ (kJ/kg), was calculated by using the slope of q vs $\dot{m}$ plot. The specific heat (c) was calculated by using the ratio of specific energy and temperature difference.

2.3.5. Temperature Profile. To model the temperature profile of the material, the net heat supplied heat capacity and moisture content are needed. The net heat supplied is defined as the difference between heat supplied with the material flow and heat losses to the surrounding. The heat losses were calculated as follows: (a) the system was heated until the steady-state temperature was reached with the temperature within ±0.5 °C; (b) after reaching the steady-state condition, the heater duty cycle (DC), defined as the "on" time of the heater ranging from 0 to 100%, was recorded; (c) heat lost to the surrounding was calculated by multiplying the duty cycle and the capacity of the heat (kW). The material was then flown into the system. After achieving the DC steady-state condition, the heat supplied to the material was calculated by measuring the DC and multiplying it with the heater capacity (kW) similar to the calculation of the heat losses. Based on the moisture content, the sensible and latent heat absorbed by the water was subtracted to convert the net heat supplied to a moisture-free (MF) basis. The material temperature was then calculated via eq 3

$$T_{material} = T_{set\ point} - \frac{\dot{m}c}{q} \tag{3}$$

where $\dot{m}$ is the material flow rate (kg/s), c is the heat capacity of the material (kJ/(kg °C)), and q (W) is the net heat supplied on a moisture-free basis.

2.3.6. Overall Heat Transfer Coefficient. The overall heat transfer coefficient (U) for combined modes of heat transfer is measured in this study. The general definition of heat transfer coefficient is given by eq 4

$$U = \frac{q''}{\Delta T} \tag{4}$$

where q'' is heat flux (W/m^2), U is average overall heat transfer coefficient (W/(m^2 K)), and ΔT (°C) is the difference in temperature between the reactor surface and the material. The overall heat transfer coefficient was measured by plotting q'' against the temperature difference. The slope of the plot indicates the value of U.

2.3.7. Specific Mechanical Energy. It is defined as energy divided by output rate as explained in eq 5.

$$\text{SME} = \frac{P}{\dot{m}} \tag{5}$$

where SME is the specific mechanical energy (kWh/t), P is the drive motor power (kW), and $\dot{m}$ is the throughput (kg/t).

2.4. Material Characterization. *2.4.1. Thermomechanical Analysis (TMA).* TMA of the produced pellets was performed by using a PerkinElmer Model TMA 7 instrument on sliced discs (0.5 mm × ϕ 9 mm) from the extruded rod using the penetration probe (static force 10 mN) from 30 to 200 °C at 5 °C/min. Data were analyzed by using Pyris v8 software to determine the onset softening temperature.

2.4.2. Flexural Testing. The extruded pellet samples and LDPE, HDPE, and PP reference materials were hot-pressed (PHI hydraulic press, 300 × 300 mm^2) slowly at 140 °C (180 °C for PP) over 20 min to a thickness of 3.25 mm and then cooled to room temperature under load. The flattened material was cut into flexural specimens of size 3.25 mm × 16 mm × 60 mm. Three-point flexural tests (strength and modulus) were performed on the specimens (≥6 replicates) according to Standard D 790-07 with a crosshead speed of 1.31 mm/min and a span of 52 mm, tested until specimen failure or 5% strain, whichever occurred first on an Instron 5500R-1132 universal test

https://doi.org/10.1021/acs.energyfuels.1c01836
Energy Fuels 2021, 35, 12227−12236

machine (5 kN load cell). Data were collected and processed by using Bluehill v3 software (Instron).

2.4.3. Dynamic Rheological Testing. Dynamic rheological measurements (storage modulus (G'), viscous modulus (G''), and complex viscosity (η^*)) were performed on the produced pellets by using a Bohlin CVO 100 rheometer, with serrated parallel plates (25 mm ϕ), in an oscillating mode with an extended temperature control module on pressed disc (3 mm × 25 mm ϕ) samples. Experiments were performed in the linear viscoelastic region. Measurements were performed at a temperature of 180 °C within a frequency range of 0.01−100 Hz at an applied strain of 0.5%.[42] Data were analyzed by using Bohlin rheology v6.51 software.

2.4.4. Pellet Durability Index. The pellet durability index (PDI) measurement was carried according to the "ASAE Pellet Durability Test Standard S269.5" and "ASTM E11-87 specification for wire-cloth sieves for testing". The pellet durability tester used was supplied by Seedburo Equipment Co.[43] The equipment consists of a box with four compartments in series, each measuring 305 mm × 305 mm × 127 mm and a 229 mm × 51 mm plate fixed symmetrically on one side. To measure the PDI index, the pellets were first sieved by using an 11.1 mm screen to ensure no fines are present in the pellets. 500 g of fines-free pellets was then tumbled in the PDI tester for 10 min at 50 rpm. The pellets were then screen by using an 11.1 mm screen, and the weight of fines-free pellets was measured. PDI was calculated via eq 6.

$$\text{PDI} = \frac{\text{wt of pellets after tumbling (g)}}{\text{wt of pellets before tumbling (g)}} \times 100 \quad (6)$$

3. RESULTS AND DISCUSSION

Figure 4 shows the FTIR results performed on the feedstock to identify its various constituents, showing various fibers and plastics. The major components are (a) LDPE, (b) PP, (c) PET, (d) polyamide nylon, (e) polyvinyl, (f) Silopren, (g) acrylate, (h) cellophane, and (i) polyester with kaolin filler. The individual IR spectra were obtained by testing multiple individual pieces, randomly picked up from the waste feedstock, and then scanning them through the infrared spectrometer.

Figure 5 shows the mass flow rate vs the feed auger rotation frequency. The mass flow rate was measured for 0 to 16 rpm of

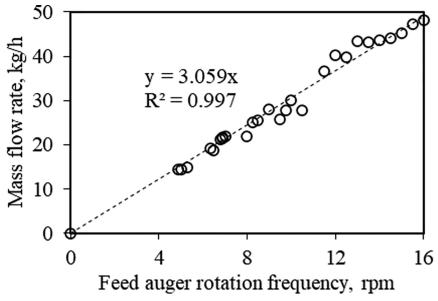

Figure 5. Mass flow rate vs feed auger rotation frequency.

the feed auger rotation frequency. Even though the material was inhomogeneous due to shredding and preprocessing, the dosing system was able to dose the material at a very consistent feed rate for the batch. The correlation found was mass flow rate (kg/h) = 3.059 × feed auger rotation frequency (rpm). The R^2 value was 0.997.

Figure 6 shows the thermal dynamics of the system. The set point is set at 300 °C, and the ramp-up time was set at 4 h. For clarity, the thermal dynamics of only one heater are shown. Note that similar dynamics are observed in all heaters. Some

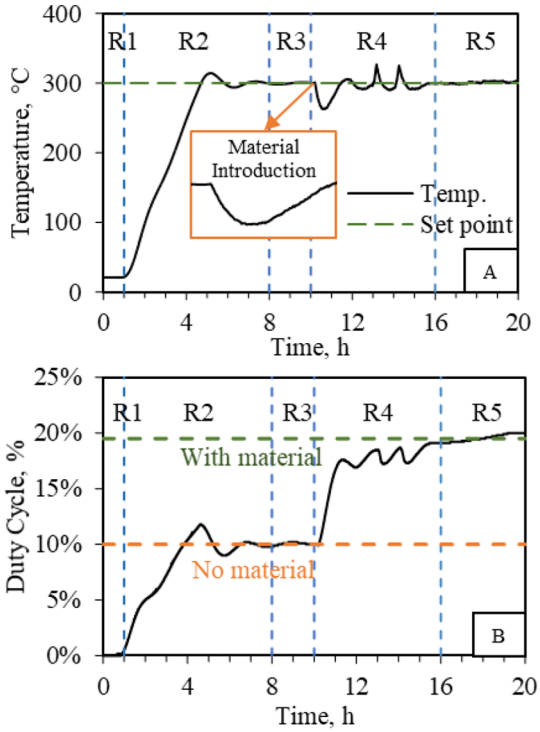

Figure 6. Thermal dynamics of the system showing five regions (R1, no heating region; R2, ramp-up region; R3, stability without material region; R4, material flow startup region; R5, stability region) with material for (A) temperature of the system and (B) DC of the heaters.

differences are observed due to the location and intercompensation of neighboring heaters. The temperature and the heater DC response can be distributed into five regions. In region R1, the system is at room temperature, and the DC of the heater is at 0% as the heaters are not operating. After the heaters are turned on, as shown in region R2, the heaters ramp up the temperature at a rate corresponding to the ramp-up timer. The PID controller parameters govern the response of the heater to the temperature change. Longer ramp-up time allows for lesser temperature overshoot and undershoot.

After the set temperatures are reached, the DC of the heater stabilizes (10% in this case) the system which is maintained at the same temperature for at least an additional 2 h to allow every part of the reactor to have a uniform temperature. The next step is to flow the material inside the reactor. As shown by region R4, as the material is introduced in the reactor, the temperature drops (Figure 6A, inset), and the DC of the heaters increases. Some start-up instabilities are observed due to the start-up procedure and approach a steady-state condition later. After the entry into region R5, the heater's duty cycles and the temperatures continue toward stability, and both the curves flattened. The source of instabilities in the duty cycle is due to the heater control system (PID control) trying to compensate for the temperature changes caused when there was a flow of material. In the 12 and 16 h regions, the fluctuations result from over- and undercompensation resulting from the PID controller that regulates the heater.

Figure 7A shows the residence time measurement vs inverse shaft speed of two different cut auger (paddle) reactor configurations in comparison to the auger configuration without any cuts/paddles. The first paddle configuration consists of 20% cuts while the second consists of 40% cuts.

https://doi.org/10.1021/acs.energyfuels.1c01836
Energy Fuels 2021, 35, 12227−12236

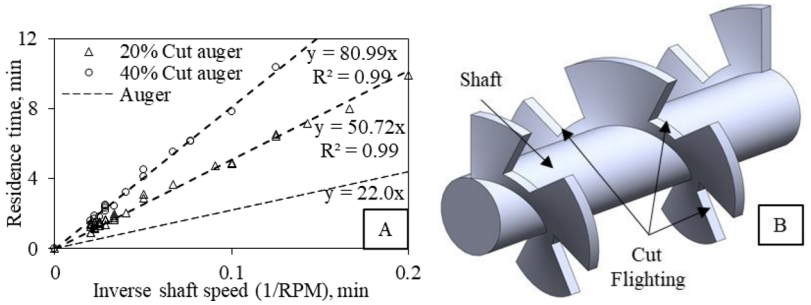

Figure 7. (A) Residence time vs inverse shaft speed for different shaft configurations (auger: 0% cut, 20% cut auger, and 40% cut auger). (B) SolidWorks model showing modified auger with 40% cuts.

Figure 7B shows a SolidWorks model showing the 40% cut section of the modified paddle configuration. It was found that the auger with no cuts has a slope of 22 (unitless) while the paddle and cut paddles have a slope of 50.7 and 81.0, respectively, showing 2.3 and 3.7 times increase in the residence times at given speed compared to the auger. The increase of residence time is due to the conveying inefficiency introduced by the cut auger design. The cut reduces the mass flow rate but allows to increase the residence time significantly in the same length of the reactor. This also increases the volume of the material inside the reactor allowing a higher fill rate (volume fraction).

Figure 8 shows the average net heat input on a moisture-free basis vs the mass flow rate. The specific heat (C) of material

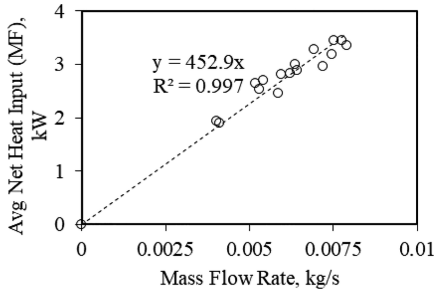

Figure 8. Average net heat input (moisture-free basis) vs mass flow rate. Specific heat (C) of material can be calculated as 1.58 kJ/(kg °C).

can be calculated by using the ratio of (average net heat input/mass flow rate) and ΔT as per eq 2. The temperature difference, ΔT, in this study is 285 °C (environment temperature was measured at 15 °C). The slope of the plot is equal to 453 kJ/kg with an R^2 of 0.997. Considering the temperature difference, the value of the specific heat for the mixed blend used can be calculated as 1.58 kJ/(kg °C). This value of specific heat is in line with the range of specific heat values measured by other studies.

We calculated the temperature profile in the reactor as explained in section 2.3.5; the temperature profile depends on mass flow rate, material and thermal properties, and reactor heat transfer coefficient. Results shown in Figure 9 are for the mass flow rate of 22.5 kg/h. It can be observed that the temperature reached 100 °C in about 0.5 min, followed by 0.2 min of constant temperature due to the water phase transition from liquid to vapor. The temperature then continues to rise further until 300 °C. The maximum residence time in the reactor is 3.3 min at 22.5 kg/h.

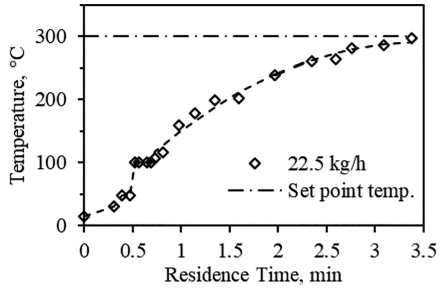

Figure 9. Material temperature profile vs residence time.

Figure 10 shows the measured value of the U based on the slope of heat flux and temperature difference between the

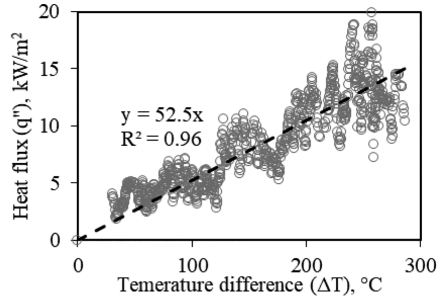

Figure 10. Average heat transfer coefficient (U) based on the slope of heat flux vs ΔT plot.

material and the set point. A large scatter is observed in the measurement due to the dynamic nature of the heater duty cycle and the strong sensitivity of the heat transfer coefficient on the heat flux. As seen from the plot, the average value of U ranges from 35 to 70 W/(m^2 °C) with an average value at 52.5 W/(m^2 °C). This value is in line with the universal heat transfer coefficient value range of 46−350 W/(m^2 °C) reported in the literature for screw reactors.

Figure 11 shows the plot of specific mechanical energy vs the mass flow rate. It can be observed that specific mechanical energy is high around 335 kWh/t at 9 kg/h, and it drops to 90 kWh/t close to 50 kg/h. It is anticipated to go down further as the mass flow rate is increased and then start increasing again as more material is pushed into the reactor than its handling capacity. The specific mechanical energy goes down with the increase in mass flow rate and can be attributed to friction.

Figure 12 shows the pellet extruded from the fiber−plastic waste material (pellets of 12.7 mm D and 25.4 mm L). The pellets had color ranging from light gray to black depending on the extent of torrefaction. In the fiber−plastic blend pellets,

https://doi.org/10.1021/acs.energyfuels.1c01836
Energy Fuels 2021, 35, 12227−12236

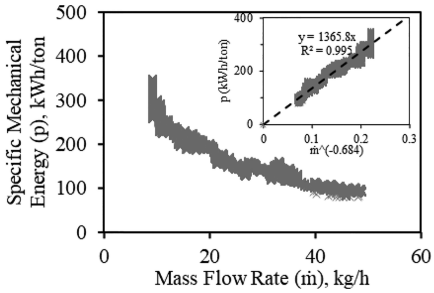

Figure 11. Specific mechanical energy (SME) vs mass flow rate of the torrefaction−extrusion process. The inset shows the plot of $\dot{m}^{-0.684}$ vs SME.

Figure 12. Pellets produced from fiber−plastic mix waste (60:40 ratio) of ϕ 12.7 mm diameter and 25.4 mm length.

plastic acted as a binder and encapsulated the fibrous material to form more consistent and uniform pellets which were consistent with our previous study.[10] The produced pellets have a good surface finish and good water resistance.[10] To address the homogeneity of the pellets, infrared spectroscopy was performed for both the feedstock and the pellets to quantify the change in degree of heterogeneity of feedstock due to the compounding process in the production of pellets. Figure S1 shows (a) 30 IR overlapping spectra of as-is material, (b) 30 IR spectra after the homogenization, and (c) comparison of the average of 30 spectra before the process and after the process. Figure S1a shows the spectra of various different materials in the feedstock appearing distinctly; this shows that feedstock was heterogeneous in nature. Figure S1b shows that all 30 spectra of pellets overlapped with each other, which indicates that the material was homogenized and appears as a single spectrum. Figure S1c shows the comparison of the average of the 30 spectra before and after the extrusion process; the spectra are almost identical, thus showing the homogeneous nature of produced pellets.

Figure 13 shows the TMA results for the pellets. Two softening temperatures, T_{s1} and T_{s2}, were observed at 102 and 164 °C. These two temperatures correspond to the melting temperature of LDPE (98−115 °C) and PP (160−175 °C), respectively. The behavior of TMA softening temperatures shown in Figure 13 corresponds only to "major" plastic components in the extruded blend, hence observing only PE and PP. As this waste stream comprises mostly mixed plastic

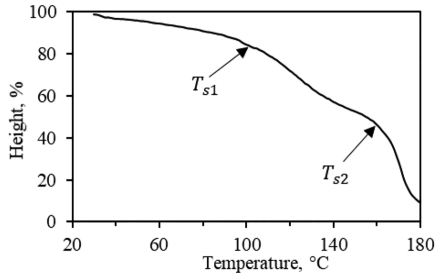

Figure 13. Thermomechanical analysis thermogram of extruded pellets showing two softening temperatures at 102 and 164 °C.

and fiber wastes, various plastic components melt in the range 120−300 °C. The reactor temperature reaches 300−400 °C, which means that the plastic components melt within the reactor. However, the fiber component does not melt. As the plastic components melt, they incapsulate the fiber particles and generate a rather homogeneous blend. This blend undergoes chemical degradation. Approaching the outlet of the extruder where the temperatures are in the range 150−170 °C the blend solidifies.

The extruded mixed plastic−fiber pellets were compression-molded into specimens and tested for their flexural properties (strength and modulus), with example results shown in Table 1. The mean flexural modulus was 1400 MPa, and the mean

Table 1. Flexural Modulus and Strength Values of Extruded Mixed Plastic−Paper, LDPE, HDPE, and PP

material	flexural modulus (MPa)	flexural strength (MPa)
mixed plastic−fiber	1400 ± 94	10.67 ± 0.77
LDPE	213 ± 36	7.14 ± 0.75
HDPE	1047 ± 42	27.4 ± 0.6
PP	1423 ± 34	36.9 ± 0.4

flexural strength was 10.7 MPa. For comparison, flexural properties of compression-molded LDPE, HDPE, and PP are given in Table 1. The mixed plastic−fiber material has a flexural modulus comparable to PP and strength comparable to LDPE.

Dynamic rheological measurement was also obtained on the extruded torrefied pellets. Figure 14 shows the results for complex viscosity (η^*) as a function of viscosity at 180 °C. The η^* is seen decreasing with the increase of angular frequency showing shear thinning behavior. For example, the η^* at 1 and 30 Hz was 16800 and 738 Pa·s, respectively. Similar behavior has been observed in reprocessed plastic wastes[10] and plastic−fiber wastes.[44]

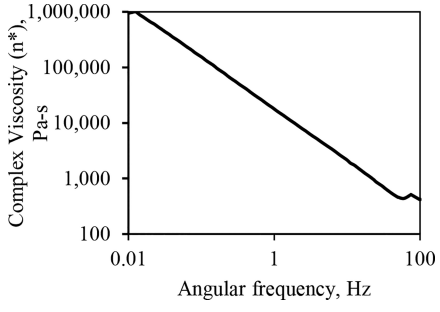

Figure 14. Flow curves showing complex viscosity vs shear rate of plastic waste at 180 °C.

https://doi.org/10.1021/acs.energyfuels.1c01836
Energy Fuels 2021, 35, 12227−12236

The pellet durability index (PDI) measurement was measured for five samples of 500 g each. The average pellet durability index was 98.27 ± 0.56%. This index indicates the high durability of pellets and minimum fines production.

To ensure the robustness of the process in treating different feedstocks, we also investigated other feedstocks, such as mixed plastic wastes, MRF residues, and so on, and have successfully obtained good results both for the process and product characteristics. The results for other waste streams and detailed analysis of these materials will be presented in future studies.

4. CONCLUSION

Torrefaction of mixed fiber−plastic sourced from industrial wastes was performed at 300 °C in an integrated torrefaction−extrusion screw reactor with a throughput of up to 70 kg/h. The study experimentally measured thermomechanical properties of both the process and the pellets produced. The residence time for the reactor was measured, and it was found that 20% and 40% cut flighting had about 2.3 and 3.7 times, respectively, more residence time compared to regular screw. The average overall heat transfer coefficient was measured experimentally for the reactor at 52.5 W/(m^2 °C). The correlation between specific mechanical energy and mass flow showed a more than 3 times decrease in specific energy consumed when feed rate was increased from ∼10 to 50 kg/h. TMA, flexural testing, rheological, and pellet durability testing were performed on the produced pellets to measure pellet properties showed that the pellet had good processability and mechanical properties (durable). In conclusion, the system can produce high-quality torrefied pellets with low specific energy costs.

■ ASSOCIATED CONTENT

Supporting Information

The Supporting Information is available free of charge at https://pubs.acs.org/doi/10.1021/acs.energyfuels.1c01836.

Appendix I includes (a) FTIR spectral comparison for mixed plastic wastes showing homogenization, (b) proximate, ultimate, and ash analysis for feedstock, (c) proximate analysis of torrefied pellets, and (d) specific power consumption comparison (PDF)

■ AUTHOR INFORMATION

Corresponding Author

Ezra Bar-Ziv − *Department of Mechanical Engineering−Engineering Mechanics, Michigan Technological University, Houghton, Michigan 49931, United States;* orcid.org/0000-0003-1444-123X; Phone: +1 906-487-3151; Email: ebarziv@mtu.edu

Authors

Shreyas S. Kolapkar − *Department of Mechanical Engineering−Engineering Mechanics, Michigan Technological University, Houghton, Michigan 49931, United States;* orcid.org/0000-0002-0474-8038

Stas Zinchik − *Department of Mechanical Engineering−Engineering Mechanics, Michigan Technological University, Houghton, Michigan 49931, United States*

Zhuo Xu − *Department of Mechanical Engineering−Engineering Mechanics, Michigan Technological University, Houghton, Michigan 49931, United States*

Armando G. McDonald − *Department of Forest, Rangeland and Fire Sciences, University of Idaho, Moscow, Idaho 83844, United States;* orcid.org/0000-0001-5877-4082

Complete contact information is available at: https://pubs.acs.org/10.1021/acs.energyfuels.1c01836

Author Contributions

S.S.K.: methodology, investigation, writing of the original draft. S.Z.: investigation, writing−review and editing. Z.X.: investigation, writing−review and editing. A.M.: supervision, investigation, writing−review and editing. E.B.-Z.: conceptualization, supervision, investigation, writing−review and editing. All authors have approved the final version of the manuscript.

Notes

The authors declare no competing financial interest.

■ ACKNOWLEDGMENTS

We acknowledge the support from (1) National Science Foundation Grant 1827364; (2) U.S. Department of Energy, Office of Energy Efficiency and Renewable Energy (EERE), Bioenergy Technologies Office (BETO), under DOE Idaho Operations Office Contract DE-AC07-05ID14517; and (3) Michigan Translational Research and Commercialization (MTRAC) program by the State of Michigan, Grant RC109248.

■ REFERENCES

(1) US Environmental Protection Agency. Advancing Sustainable Materials Management: 2017 Fact Sheet, 2019.

(2) Thompson, J. US landfill capacity to drop 15% over next 5 years; https://wihresourcegroup.wordpress.com/2018/06/20/us-landfill-capacity-to-drop-15-over-next-5-years/ (accessed 2021-09-03).

(3) Kantner, D.; Staley, B. EREF: Analysis of MSW Landfill Tipping Fees April 2019, 2019; www.erefdn.org.

(4) Brooks, A. L.; Wang, S.; Jambeck, J. R. The Chinese Import Ban and Its Impact on Global Plastic Waste Trade. *Sci. Adv.* **2018**, *4* (6), No. eaat0131.

(5) Katx, C. Piling Up: How China's Ban on Importing Waste Has Stalled Global Recycling; https://e360.yale.edu/features/piling-up-how-chinas-ban-on-importing-waste-has-stalled-global-recycling (accessed 2021-07-05).

(6) Truelove, A.; Katan, C. The State of Recycling National Survey - U.S. PIRG Education Fund; https://uspirg.org/sites/pirg/files/reports/Trash-In-America/The-State-of-Recycling-National-Survey_111319.pdf (accessed 2021-06-07).

(7) U.S Department of Energy: EERE. Waste-to-Energy from Municipal Solids Wastes; https://www.energy.gov/sites/prod/files/2019/08/f66/BETO--Waste-to-Energy-Report-August--2019.pdf.

(8) Abdul Samad, N. A. F.; Jamin, N. A.; Saleh, S. Torrefaction of Municipal Solid Waste in Malaysia. *Energy Procedia* **2017**, *138*, 313−318.

(9) Koppejan, J.; Sokhansanj, S.; Melin, S.; Madrali, S. *Status Overview of Torrefaction Technologies*; IEA Bioenergy: 2015.

(10) Zinchik, S.; Xu, Z.; Kolapkar, S. S.; Bar-Ziv, E.; McDonald, A. G. Properties of Pellets of Torrefied U.S. Waste Blends. *Waste Manage.* **2020**, *104*, 130−138.

(11) Campuzano, F.; Brown, R. C.; Martínez, J. D. Auger Reactors for Pyrolysis of Biomass and Wastes. *Renewable Sustainable Energy Rev.* **2019**, *102*, 372−409.

(12) de Souza, H. J. P. L.; Arantes, M. D. C.; Vidaurre, G. B.; Andrade, C. R.; Carneiro, A. de C. O.; de Souza, D. P. L.; Protásio, T. de P. Pelletization of Eucalyptus Wood and Coffee Growing Wastes: Strategies for Biomass Valorization and Sustainable Bioenergy Production. *Renewable Energy* **2020**, *149*, 128−140.

(13) Setkit, N.; Li, X.; Yao, H.; Worasuwannarak, N. Torrefaction Behavior of Hot-Pressed Pellets Prepared from Leucaena Wood. *Bioresour. Technol.* **2021**, *321*, 124502.
(14) Martínez, I.; Grasa, G.; Callén, M. S.; López, J. M.; Murillo, R. Optimised Production of Tailored Syngas from Municipal Solid Waste (MSW) by Sorption-Enhanced Gasification. *Chem. Eng. J.* **2020**, *401* (May), 126067.
(15) EERE, U. S. D. of E. Alternative Aviation Fuels: Overview of Challenges, Opportunities, and Next Steps, 2021; Vol. DOE/EE-151.
(16) Convergen-Energy. Renewable & sustainable fuel https://www.convergenenergy.com/our-fuels/ (accessed 2021-03-06).
(17) Pellet America Corp. Renewable energy - recycled fuel pellets http://www.pelletamerica.com/ (accessed 2021-03-06).
(18) Kwon, W. T.; Bae, S. Y. Utilization of Waste Plastics as a Fuel in the Fluidized Bed Calciner for Cement Kiln Process. *Mater. Sci. Forum* **2005**, *486*−*487*, 399−402.
(19) Laucks, I. F. The Screw as a Carbonizing Machine. *Ind. Eng. Chem.* **1927**, *19* (1), 9−11.
(20) Kelkar, S.; Saffron, C. M.; Chai, L.; Bovee, J.; Stuecken, T. R.; Garedew, M.; Li, Z.; Kriegel, R. M. Pyrolysis of Spent Coffee Grounds Using a Screw-Conveyor Reactor. *Fuel Process. Technol.* **2015**, *137*, 170−178.
(21) Atienza-Martínez, M.; Mastral, J. F.; Ábrego, J.; Ceamanos, J.; Gea, G. Sewage Sludge Torrefaction in an Auger Reactor. *Energy Fuels* **2015**, *29* (1), 160−170.
(22) Zinchik, S.; Klinger, J. L.; Westover, T. L.; Donepudi, Y.; Hernandez, S.; Naber, J. D.; Bar-Ziv, E. Evaluation of Fast Pyrolysis Feedstock Conversion with a Mixing Paddle Reactor. *Fuel Process. Technol.* **2018**, *171*, 124−132.
(23) Brown, J. N. *Development of a Lab-Scale Auger Reactor for Biomass Fast Pyrolysis and Process Optimization Using Response Surface Methodology*, Iowa State University, 2009.
(24) Recari, J.; Berrueco, C.; Puy, N.; Alier, S.; Bartrolí, J.; Farriol, X. Torrefaction of a Solid Recovered Fuel (SRF) to Improve the Fuel Properties for Gasification Processes. *Appl. Energy* **2017**, *203*, 177−188.
(25) Daniel, J.; Murillo, R.; García, T.; Veses, A. Demonstration of the Waste Tire Pyrolysis Process on Pilot Scale in a Continuous Auger Reactor. *J. Hazard. Mater.* **2013**, *261*, 637−645.
(26) Brown, J. N.; Brown, R. C. Process Optimization of an Auger Pyrolyzer with Heat Carrier Using Response Surface Methodology. *Bioresour. Technol.* **2012**, *103* (1), 405−414.
(27) Xu, Z.; Zinchik, S.; Kolapkar, S. S.; Bar-Ziv, E.; Hansen, T.; Conn, D.; McDonald, A. G. Properties of Torrefied U.S. Waste Blends. *Front. Energy Res.* **2018**, *6* (July), 1−13.
(28) Xu, Z.; Albrecht, J. W.; Kolapkar, S. S.; Zinchik, S.; Bar-Ziv, E. Chlorine Removal from U.S. Solid Waste Blends through Torrefaction. *Appl. Sci.* **2020**, *10* (9), 3337.
(29) Shi, X.; Ronsse, F.; Nachenius, R.; Pieters, J. G. 3D Eulerian-Eulerian Modeling of a Screw Reactor for Biomass Thermochemical Conversion. Part 2: Slow Pyrolysis for Char Production. *Renewable Energy* **2019**, *143*, 1477−1487.
(30) Qi, F.; Wright, M. M. A DEM Modeling of Biomass Fast Pyrolysis in a Double Auger Reactor. *Int. J. Heat Mass Transfer* **2020**, *150* (2), 119308.
(31) Funke, A.; Grandl, R.; Ernst, M.; Dahmen, N. Modelling and Improvement of Heat Transfer Coefficient in Auger Type Reactors for Fast Pyrolysis Application. *Chem. Eng. Process.* **2018**, *130*, 67−75.
(32) Qi, F.; Wright, M. M. Particle Scale Modeling of Heat Transfer in Granular Flows in a Double Screw Reactor. *Powder Technol.* **2018**, *335*, 18−34.
(33) Waje, S. S.; Thorat, B. N.; Mujumdar, A. S. An Experimental Study of the Thermal Performance of a Screw Conveyor Dryer. *Drying Technol.* **2006**, *24* (3), 293−301.
(34) Godavarti, S.; Karwe, M. V. Determination of Specific Mechanical Energy Distribution on a Twin-Screw Extruder. *J. Agric. Eng. Res.* **1997**, *67* (4), 277−287.
(35) Berzin, F.; Tara, A.; Tighzert, L.; Vergnes, B. Importance of Coupling between Specific Energy and Viscosity in the Modeling of Twin Screw Extrusion of Starchy Products. *Polym. Eng. Sci.* **2010**, *50* (9), 1758−1766.
(36) Schmid, V.; Steck, J.; Mayer-Miebach, E.; Behsnilian, D.; Bunzel, M.; Karbstein, H. P.; Emin, M. A. Extrusion Processing of Pure Chokeberry (Aronia Melanocarpa) Pomace: Impact on Dietary Fiber Profile and Bioactive Compounds. *Foods* **2021**, *10* (3), 518.
(37) Sasimowski, E.; Majewski, Ł.; Grochowicz, M. Efficiency of Twin-Screw Extrusion of Biodegradable Poly (Butylene Succinate)-Wheat Bran Blend. *Materials* **2021**, *14* (2), 424.
(38) Lepschi, A.; Gerstorfer, G.; Miethlinger, J. Determining the Residence Time Distribution of Various Screw Elements in a Co-Rotating Twin-Screw Extruder by Means of Fluorescence Spectroscopy. *AIP Conf. Proc.* **2014**, *1664*, 020005.
(39) Nikitine, C.; Rodier, E.; Sauceau, M.; Fages, J. Residence Time Distribution of a Pharmaceutical Grade Polymer Melt in a Single Screw Extrusion Process. *Chem. Eng. Res. Des.* **2009**, *87* (6), 809−816.
(40) Xu, Z.; Kolapkar, S. S.; Zinchik, S.; Bar-Ziv, E.; McDonald, A. G. Comprehensive Kinetic Study of Thermal Degradation of Polyvinylchloride (PVC). *Polym. Degrad. Stab.* **2020**, *176*, 109148.
(41) Giles, H. F., Jr.; Wagner, J. R., Jr.; Mount, E. M., III *Extrusion: The Definitive Processing Guide and Handbook*, 1st ed.; William Andrew Publishing: Norwitch, NY, 2005.
(42) Luo, S.; Cao, J.; McDonald, A. G. Interfacial Improvements in a Green Biopolymer Alloy of Poly(3-Hydroxybutyrate-Co-3-Hydroxyvalerate) and Lignin via in Situ Reactive Extrusion. *ACS Sustainable Chem. Eng.* **2016**, *4* (6), 3465−3476.
(43) Stark, C.; Fahrenholz, A. Evaluating Pellet Quality. *Kansas State Univ. Agric. Exp. Stn. Coop. Ext. Serv.* **2015**, *ME3228*, 0−3.
(44) Xu, Z.; Kolapkar, S. S.; Zinchik, S.; Bar-Ziv, E.; Ewurum, L.; McDonald, A. G.; Klinger, J.; Fillerup, E.; Schaller, K.; Pilgrim, C. Bypassing Energy Barriers in Fiber-Polymer Torrefaction. *Front. Energy Res.* **2021**, *9* (March), 1−13.

https://doi.org/10.1021/acs.energyfuels.1c01836
Energy Fuels 2021, 35, 12227−12236